# Radiative recombination properties of near-stoichiometric $CuInSe_2$ thin films

S. Levcenko,[1,*] H. Stange,[1,2] L. Choubrac,[1] D. Greiner,[3] M. D. Heinemann,[3] R. Mainz,[1] and T. Unold[1]

[1]*Helmholtz-Zentrum für Materialien und Energie, Hahn-Meitner-Platz 1, 14109 Berlin, Germany*

[2]*Technische Universität Berlin, Institut für Werkstoffwissenschaften, 10587 Berlin, Germany*

[3]*PVcomB/Helmholtz-Zentrum Berlin für Materialien und Energie, Schwarzschildstrasse 3, 12489 Berlin, Germany*

(Received 5 March 2020; accepted 29 May 2020; published 24 June 2020)

The properties of electronic defects and their relation to structural defects are of high relevance for $CuInSe_2$ photovoltaic absorbers. Here, we use Raman scattering and steady-state photoluminescence to study the intrinsic optoelectronic properties of near-stoichiometric $CuInSe_2$ samples with a lateral composition gradient around the Cu saturation point. Apart from a well-known shallow defect band at 0.97 eV, we also observe a deep defect band at 0.8 eV, which is not discernable in photoluminescence spectra at lower temperatures. The preparation of a laterally graded sample with a very precise relative composition range by *in situ* process control allows for a measurement of a significant decrease of the photoluminescence emission yield at the Cu-poor/Cu-rich transition on a very narrow composition scale. Possible assignments of the bands to structural point defects are discussed.

DOI: 10.1103/PhysRevMaterials.4.064605

## I. INTRODUCTION

Power conversion efficiencies as high as 23.35% have been achieved for $Cu(In, Ga)Se_2$ (CIGS) chalcopyrite-type thin-film solar cells [1]. The three-stage process is one of the most developed and most studied coevaporation methods for high-quality CIGS absorbers [2,3]. This process features a sequence of three coevaporation stages: (i) In, Ga, and Se; (ii) Cu and Se; and (iii) In, Ga, and Se. During the second stage when the stoichiometric composition of CIGS is reached and the thin-film composition undergoes a chemical transition from Cu-poor ($[Cu]/([In] + [Ga]) < 1$) to Cu-rich ($[Cu]/([In] + [Ga]) > 1$), the microstructural properties of the CIGS thin films are remarkably improved [4–6]. This change in microstructure coincides with a Cu-Se secondary phase segregation at the thin-film surface. The copper deposition rate, substrate temperature, presence of sodium, and the specifics of annealing are important growth parameters which are expected to influence the thin-film microstructure and electronic properties near the Cu-poor/Cu-rich transition [4–6]. Although there have been a number of reports on grain growth, defect annihilation mechanisms, and other microstructure changes related to the Cu-poor/Cu-rich transition and their relation to structural and chemical properties [7–12], there is very little information about the optoelectronic properties of defects that might be present or formed during this process. Photoluminescence (PL) has been shown to be very sensitive to the composition of chalcopyrites, in particular, to the [Cu]/([In]+[Ga]) content [13–17]. Low-temperature PL is a powerful tool for the determination of defect signatures in chalcopyrites, and it is equally applied to the characterization of thin films and the photovoltaic devices based on them.

While previous PL studies of the recombination mechanism of $CuInSe_2$ (CIS) and CIGS show differences between Cu-poor and Cu-rich samples [13–16], they rely on samples from various processes with a broad compositional range. To investigate whether an abrupt change in the recombination mechanism occurs right at the transition from Cu-poor to Cu-rich composition, we here study the influence of the [Cu]/[In]-ratio on the optoelectronic properties of CIS in a narrow compositional region close to the point of Cu saturation marked by a Cu-Se segregation. To this end, samples with a lateral Cu gradient, including the point of Cu saturation, were produced by interrupting the coevaporation process during the Cu-Se deposition, i.e., during the second stage of the three-stage process. This provides the possibility to examine the effect of the Cu content near the Cu-poor/Cu-rich transition on the optoelectronic properties by spatially mapping Raman and temperature-dependent photoluminescence spectroscopy.

## II. EXPERIMENTAL DETAILS

We chose to study CIS samples with Cu gradients instead of CIGS samples to avoid additional In/Ga composition gradients. For the sample preparation, $In_2Se_3$ thin films were deposited at 330 °C by thermal coevaporation onto molybdenum-covered soda lime glass substrates. The substrate featured an additional $SiN_xO_y$ layer between the soda lime glass and the Mo layer, serving as a Na diffusion barrier. Subsequently, Cu-Se was evaporated onto these precursor films at 420 °C in a coevaporation chamber specifically adapted for *in situ* energy-dispersive x-ray diffraction (EDXRD) and x-ray fluorescence (XRF) measurements [18] and equipped with white-light reflectometry [7] and laser-light scattering (LLS) [19]. Optical as well as XRF and EDXRD measurement signals [5,7,9] show characteristic changes that allow the determination of the process time for which Cu saturation is achieved at a particular measuring spot, triggering the stop of the Cu deposition. Due to the relative position of the evaporation cone of the Cu source and the substrate, this procedure leads to a sample with a lateral Cu

*sergiu.levcenco@helmholtz-berlin.de

 

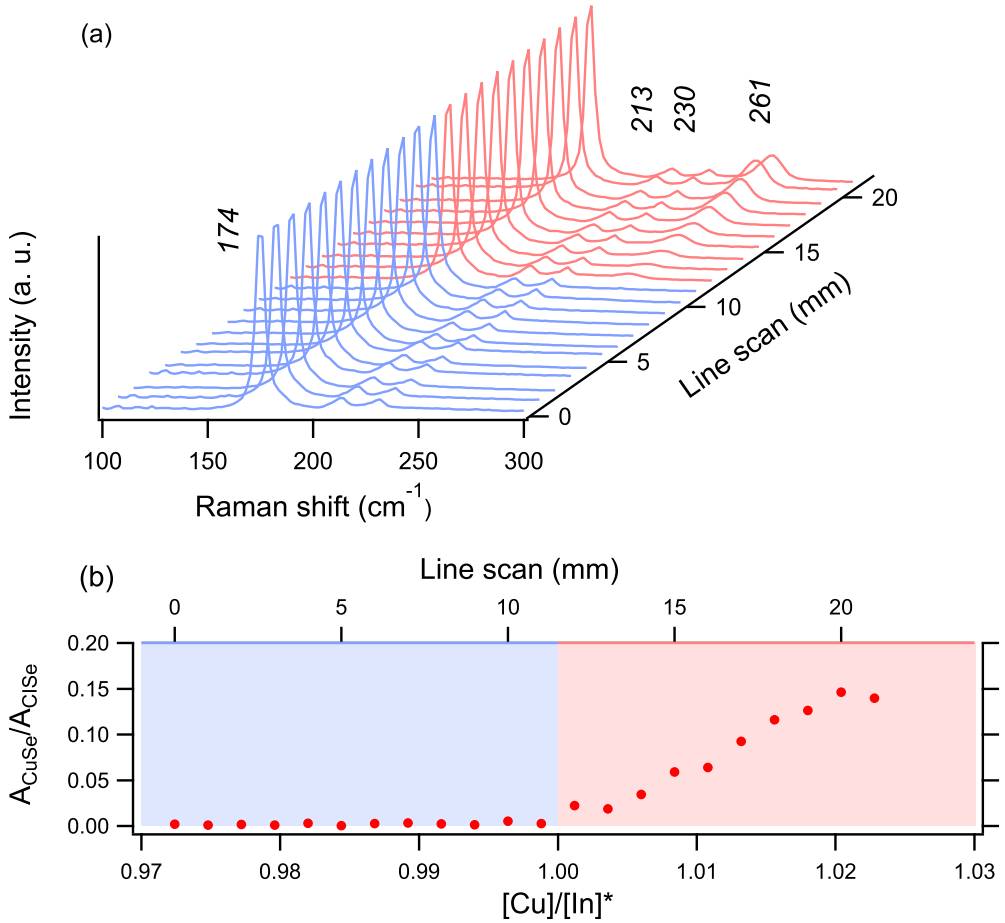


FIG. 1. (a) Line scan of micro-Raman along the copper gradient on the CIS sample. (b) Ratio of the $Cu_{2-x}Se$ peak (at 261 $cm^{-1}$) to the main CIS peak (at 174 $cm^{-1}$) along the Cu gradient. The blue and red background respectively mark the Cu-poor ([Cu]/[In]* < 1) and Cu-rich ([Cu]/[In]* > 1) sample areas.

gradient ranging from a Cu-poor to a Cu-rich composition. To improve the in-depth homogeneity of the sample, after the Cu deposition the substrate temperature was kept constant for a 10 min annealing for one type of sample before cooldown. The photoluminescence signal was measured using a 660-nm diode laser as an excitation source and detected using a 0.5-m grating monochromator coupled with a liquid-nitrogen-cooled linear InGaAs array. For temperature-dependent measurements a He closed-cycle cryogenic cryostat was used. Raman measurements were carried out at room temperature in the backscattering configuration using a Renishaw micro-Raman system with 20X objective (NA = 0.4) and a 532-nm laser.

### III. RESULTS AND DISCUSSION

To relate the optoelectronic properties with structural properties near the Cu-poor to Cu-rich transition, we carried out micro-Raman measurements on the coevaporated CIS samples with a lateral Cu gradient. Figure 1(a) shows representative line scans along the Cu gradient. Raman spectroscopy reveals the characteristic $A_1$ mode at 174 $cm^{-1}$, contributions from $E/B_2$ modes at 213 and 230 $cm^{-1}$ of chalcopyrite CIS with a tetragonal structure [20], and the presence of a $Cu_{2-x}Se$ phase (mode at 261 $cm^{-1}$) in the Cu-rich regions of the CIS film (Fig. 1(a)). We analyze the presence of a $Cu_{2-x}Se$ phase along the Cu graded samples by plotting the ratio of the Raman peak area corresponding to $Cu_{2-x}Se$ (in the 250−270 $cm^{-1}$ range) to the area corresponding to the CIS phase (in the 160−190 $cm^{-1}$ range) as shown in Fig. 1(b). We do not observe any changes in frequency or linewidth (∼6 $cm^{-1}$) of the $A_1$ chalcopyrite main mode in the probed areas of the samples. In the following, we use the onset of the $Cu_{2-x}Se$ phase Raman signal as reference for the point of Cu saturation. To calibrate the [Cu]/[In] ratio determined from the XRF (Fig. S1 of the Supplemental Material [21]), we assume that Cu saturation occurs at a ratio of [Cu]/[In] = 1. In other words, we assume that the [Cu]:[In] ratio is approximately 1:1 in the $CuInSe_2$ phase when the overall film is in the Cu-rich region. However, the Cu-Se secondary phase might not only segregate at the surface, as it was shown in Ref. [8]. To highlight the derived nature of the thus-obtained composition ratios, they are marked as [Cu]/[In]* and vary from 0.972 to 1.023.

Figure 2(a) shows the normalized PL spectra along the Cu gradient measured at 15 K and an excitation intensity of 50 $W/cm^2$. Four emission bands can be observed, with considerable changes occurring along the Cu concentration gradient. The most intense band is a narrow peak at 0.97 eV. We assign the 0.97-eV band to a donor-acceptor pair (DAP) recombination process originating from the transition

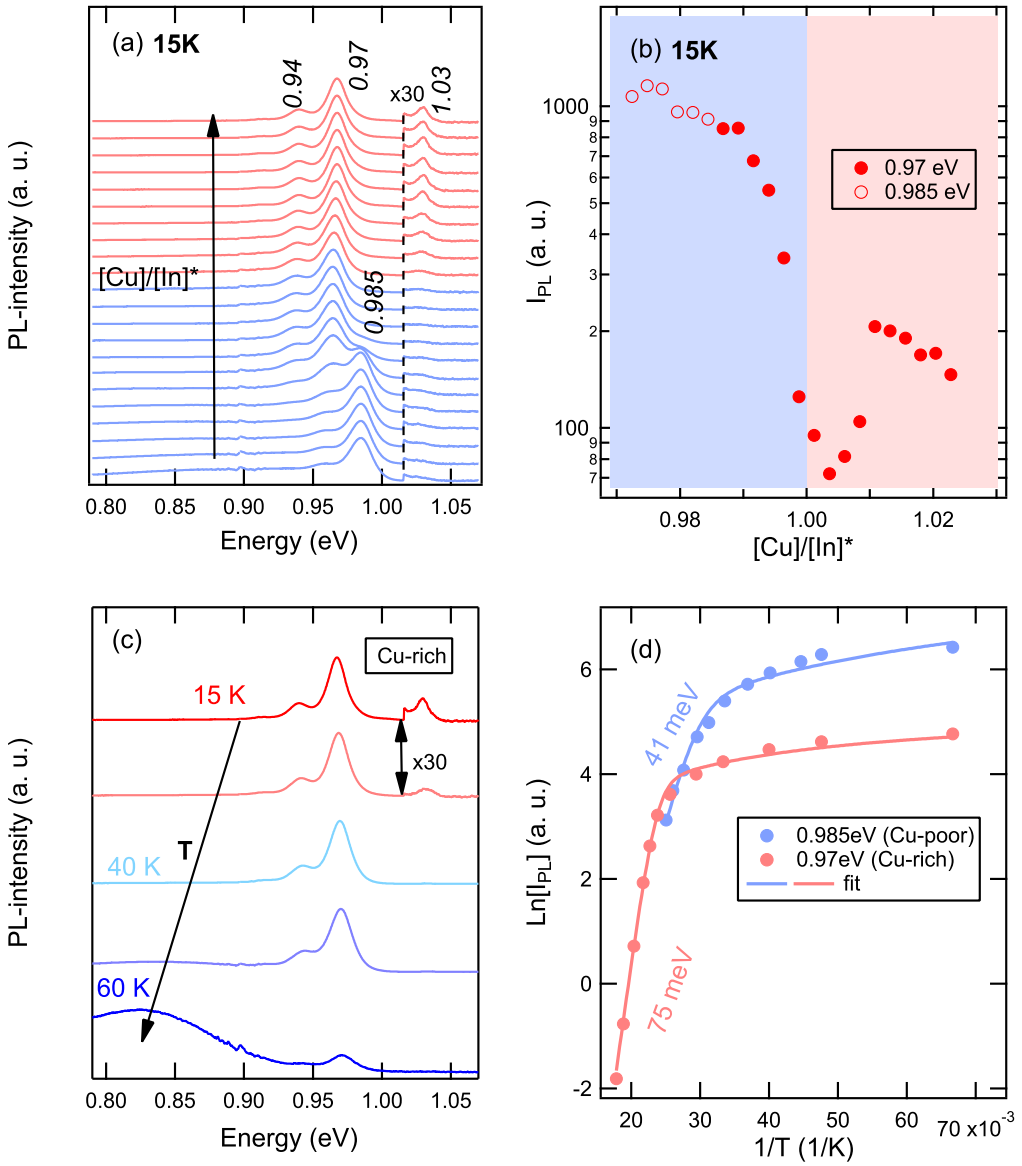


FIG. 2. (a) Normalized photoluminescence line scan and (b) PL intensity of the 0.97- and 0.985-eV bands along the Cu gradient on the CIS sample at 15 K. (c) Temperature dependence of the normalized PL spectra in the Cu-rich ([Cu]/[In]* = 1.023) area on the CIS sample. (d) Temperature quenching of the 0.985- and 0.97-eV bands in the Cu-poor ([Cu]/[In]* = 0.972) and Cu-rich ([Cu]/[In]* = 1.023) areas of the CIS sample.

between a shallow acceptor and donor [22,23], consistent with previous assignments for near-stoichiometric CIS [24,25]. For this band at 0.97 eV we measure a noticeable shift with the excitation intensity ($I_{EX}$) with a rate $\beta \approx 3$ meV/decade, and the PL intensity ($I_{PL}$) follows a power law ($I_{PL} \sim I_{EX}^{k}$) with the power coefficient $k$ of about 0.9–1 (not shown). We note that some previous reports in literature found no shift in the PL maximum with varied $I_{EX}$ for a band at 0.97 eV and have attributed this transition to a free-to-bound (FB) recombination process [13,23], which might be explained by the absence or small activation energy of the involved donor states, making the radiative recombination of a free electron and a neutral acceptor the dominant transition in those studies.

The 0.97-eV band peak position and the full width at half maximum (FWHM) are especially affected by the Cu variation: a redshift by ~4 meV (Fig. S2(a) of the Supplemental Material [21]) and a small broadening by 5 meV can be observed when the [Cu]/[In]* decreases from 1.01 to 0.99. However, the emission position and FWHM stay constant in the more Cu-rich region ([Cu]/[In]* > 1.01). Although the PL maximum position depends on the excitation power, the observed redshift of the PL is not due to the difference in the $\beta$ parameter as the Cu-poor areas show a $\beta \approx 4$ meV/decade, which is even higher than in Cu-rich areas ($\beta \approx 3$ meV/decade). We assume that a slight increase in the ionization energy of the involved donor or acceptor defect causes the redshift of the PL maximum. A reduction of the band gap with Cu deficiency in CIS could also explain the PL maximum redshift. Such a reduction has been observed for the Cu-poor side relative to stoichiometric CIS composition [26,27]. The observed saturation of the PL maximum for the Cu-poor areas can be explained by an increase of the $\beta$

parameter, which counteracts the decrease of the band gap. The emission at 0.97 eV disappears for $[Cu]/[In]^* < 0.982$ [Fig. 2(a)]. Instead, a new PL band at 0.985 eV develops for lower [Cu]/[In]* and becomes a dominant emission in the Cu-poor region [Fig. 2(a)]. This PL band shifts to high-photon energy by 3 meV/decade with increasing excitation power, and its PL intensity varies with a value of 0.7 for the $k$ coefficient (not shown). As a result, we assign the emission at 0.985 also to a DAP transition, similar to previous reports [16,24,25]. While in a previous study on epitaxial films the existence of the DAP band at 0.99 eV is observed for a [Cu]/[In] ratio ranging from 0.94 to 1.18 [25], Zott *et al.* [13] observed the 0.99-eV band only for slightly Cu-poor compositions ($[Cu]/[In] = 0.97; 0.95$) of polycrystalline thin films, which is similar to our results.

A narrow emission band at 0.94 eV [Fig. 2(a)] is attributed to a LO phonon replica of the 0.97-eV band [16,24,25], implying a phonon energy of ∼30 meV. At 100 K the highest frequency peaks in the Raman spectrum of CIS are the E(LO) and $B_2$(LO) modes, both located at 233 $cm^{-1}$ (∼ 29 meV) [20]. These modes are most likely candidates for the phonons that are involved in the 0.94-eV band. At the high-energy side of the main 0.97-eV transition, we find a very weak emission located at 1.03 eV and with a FWHM of ∼15 meV, which is more pronounced in the Cu-rich area [Fig. 2(a)]. This emission is assigned to a bound exciton recombination [28,29]. Additionally, below 0.9 eV in the PL spectra we observe a broad band at 0.87 eV. The intensity of this band decreases with Cu content increase until $[Cu]/[In]^* \sim 1.02$, when only the continuous PL background is observed (Fig. S3 of the Supplemental Material [21]).

Interestingly, the PL yield, $I_{PL}$, of the most intense 0.97- and 0.985-eV bands shows a very strong decrease with increasing Cu content in the Cu-poor range, followed by an S-shape (decrease-increase-decrease) evolution in the Cu-rich range [Fig. 2(b)], which will be further discussed below.

To study the temperature dependence of the PL signals and determine the activation energies of the main transitions, we increased the sample temperature from 15 to 60 K. Figure 2(c) shows the evolution of the PL spectra over this temperature range for a measurement at a Cu-rich composition ($[Cu]/[In]^* \sim 1.023$). The intensity of the 0.97-eV band is found to decrease strongly with rising temperature, while the weak excitonic emission at 1.03 eV is quenched even more rapidly and can be resolved only up to 30–40 K. We analyze the thermal quenching of the 0.97-eV (0.985 eV at a Cu-poor composition $[Cu]/[In]^* \sim 0.972$) transition [see Fig. 2(d)] by a model that takes into account a nonradiative process and temperature dependence of defect capture cross sections [24,30]:

$$I(T) = \frac{I_0}{1 + a_1 T^{\frac{3}{2}} + a_2 T^{\frac{3}{2}} \exp\left(-\frac{E_A}{k_B T}\right)}, \qquad (1)$$

where $I_0$ is the intensity extrapolated to $T = 0$ K, $a_1$ and $a_2$ are the process rate parameters, $k_B$ is the Boltzmann constant, and $E_A$ is the activation energy. The Arrhenius plot analysis provides an $E_A$ value of 75 meV for the 0.97-eV band at a Cu-rich composition ($[Cu]/[In]^* = 1.023$) and a smaller activation energy of $E_A = 41$ meV for the 0.985-eV band at slightly Cu-poor composition ($[Cu]/[In]^* = 0.972$). The data lie within the range of previously reported values for near-stoichiometric and Cu-rich CIS samples, with a lower activation energy for the DAP band at 0.99 eV (32–42 meV) than for the DAP band at 0.97 meV (46–66 meV) [16,24,25].

A deeper broad PL band at ∼0.8 eV is manifested in the PL spectra at 40–50 K, when the DAP transition at 0.97 eV strongly quenches [Fig. 2(c)]. With a further temperature rise to 60 K, this deep band shifts by 10–20 meV to lower energy and becomes the dominant PL recombination in the CIS samples. Line scan of the normalized PL spectra across the Cu gradient at 60 K is shown in Fig. 3(a). At stoichiometric composition, the position of the deep emission is 0.81 eV. The band position moves to higher energies for both higher and lower Cu content, by up to 35 meV for $[Cu]/[In]^* = 0.972$ and 15 meV for $[Cu]/[In]^* = 1.023$ (see Fig. S2(b) of the Supplemental Material [21]).

Similar to the behavior of the 0.97 band at 15 K [Fig. 2(b)], the PL yield, $I_{PL}$, of the ∼0.8-eV band at 60 K decreases strongly over more than a magnitude with increasing Cu content in the Cu-poor range. In the Cu-rich range a small increase is observed for the $[Cu]/[In]^* \sim 1.01$ composition [Fig. 3(b)]. At 60 K the intensity of the 0.97 emission is influenced by the high-energy shoulder of the dominating ∼0.8-eV broad band [Fig. 3(a)]. Therefore the changing intensity of the broad ∼0.8-eV emission is a possible explanation for the reemergence of the 0.97 band at slightly Cu-poor compositions in Fig. 3(a).

The analysis of the dependence of the deep band at ∼0.8-eV on the excitation intensity is complicated due to its low intensity and the spectral detection limitation of the detector. Nevertheless, for a Cu-poor ($[Cu]/[In]^* \sim 0.972$) composition, where the deep emission has the most intensive signal, it yields a value of 17 (4) meV/decade for $\beta$ at the low (high) excitation power regime, pointing to a DAP recombination mechanism (Fig. S4 of the Supplemental Material [21]). However, the observed large spectral blueshift of the PL transition significantly differs from those of the 0.97- or 0.985-eV DAP transitions, which cannot be explained with the effective mass theory based on a hydrogen model [31].

To determine the activation energy $E_{A2}$ of this deep band transition, we further increased the temperature from 60 to 225 K. In this temperature region, the deep band shifts towards lower energies [Fig. 3(c)]. At the same time, the band quenches: the intensity, calculated from the area of the visible part (photon energy range 0.79–0.95 eV) of the deep emission, decreases by two orders of magnitude as the temperature rises from 60 to 225 K.

To derive the activation energies $E_{A2}$ in the Cu-poor ($[Cu]/[In]^* \sim 0.972$) region, we apply a simple model with one nonradiative path, $I_{PL} = I_0/[1 + a_0 \exp(-E_{A2}/k_B T)]$ for the high-temperature region ($T > 90$ K), where a rapid thermal quenching occurs [Fig. 3(d)], obtaining a value of $E_{A2} \sim 150$ meV. For the Cu-rich region ($[Cu]/[In]^* \sim 1.023$) a similar analysis yields a smaller value of $E_{A2} \sim 27$ meV, indicating that the activation energy depends on the Cu content. However, due to the shift of the position of the deep band, a more accurate determination of the activation energy $E_{A2}$ would require a detector with an extension of the spectral range to photon energies below 0.79 eV. In the

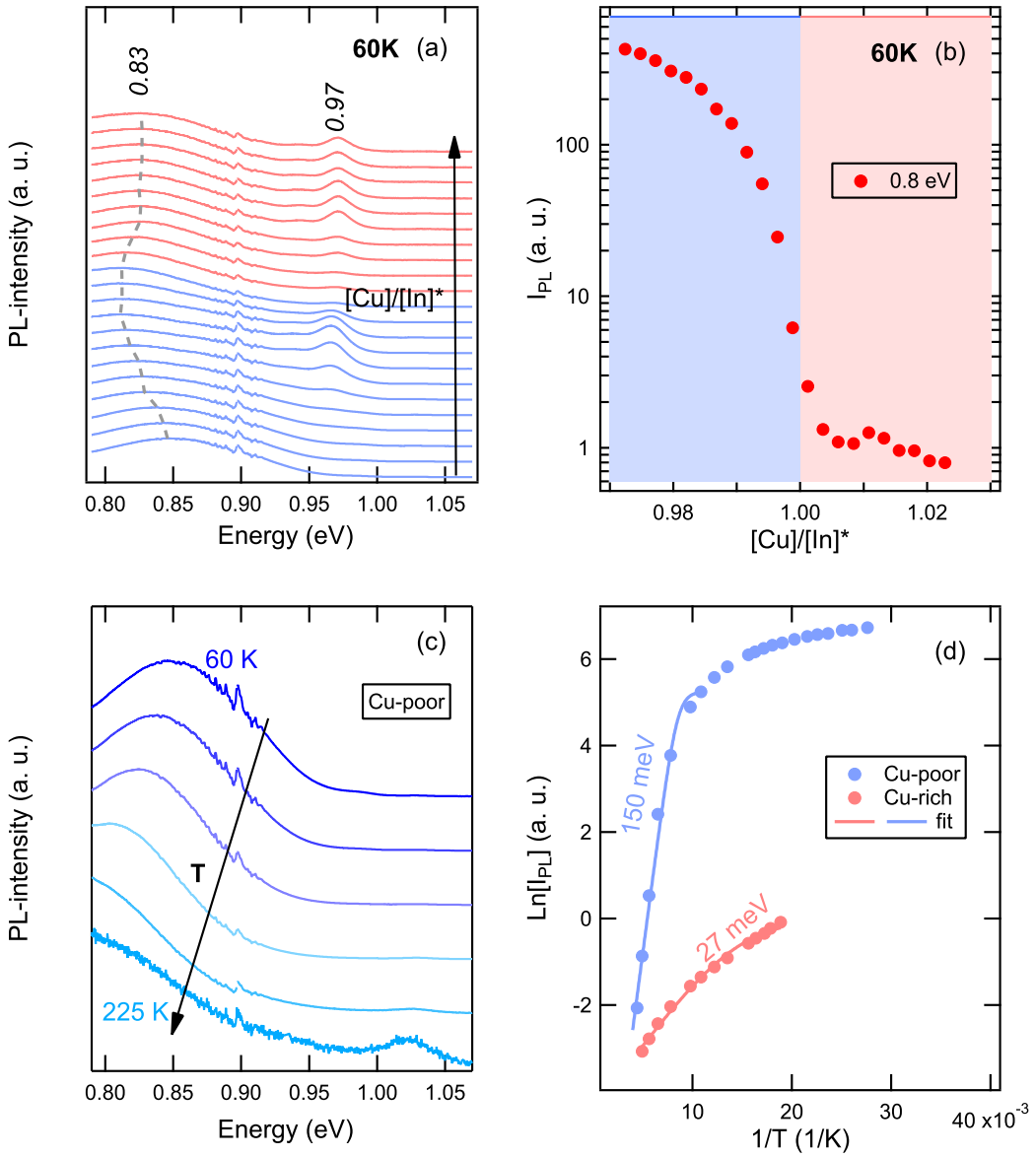


FIG. 3. (a) Normalized photoluminescence line scan and (b) PL intensity of the 0.8-eV band along the Cu gradient on the CIS sample at 60 K. The dashed gray line marks the position of the PL maximum. (c) Temperature dependence of the normalized PL spectra in the Cu-poor ([Cu]/[In]* = 0.972) area on the CIS sample. (d) Temperature quenching of the 0.85- and 0.82-eV band in the Cu-poor ([Cu]/[In]* = 0.972) and Cu-rich ([Cu]/[In]* = 1.023) areas of the CIS sample.

high-temperature region (150–300 K) a band-to-band transition at 1.02 eV becomes apparent in the Cu-rich region (Fig. S5 of the Supplemental Material [21]); however, no radiative emission is observed above 225 K in the Cu-poor region [Fig. 3(c)].

While the band at 0.97 eV (15 K) has been well studied, there are only few reports on the deep emission at ∼0.8(60 K). Earlier PL studies at 80 K showed the presence of a deep emission at about 0.8 eV in *p*-type CIS crystals [32] and in polycrystalline thin films [33], however, without an excitation- or temperature-dependent analysis. Recently, Spindler *et al.* found a deep PL band at 0.8 eV with similar excitation dependence and temperature characteristics for Cu-rich ([Cu]/[In] = 1.24) epitaxial and polycrystalline CIS films which they attribute to transitions from the deep defect state with broad distribution located about 0.8 eV above the valence band (VB) [16]. The state filling and carrier redistribution over the available states of this broad defect band are believed to explain the unusual excitation and temperature dependencies of the deep PL emission [16]. Although the behavior of this deep emission is quite complex and the actual radiative recombination mechanism is yet to be determined, we can construct at least two scenarios. Following Spindler *et al.* [16], the defect band is 0.8 eV above the VB, and relying on its donor nature we can ascribe the deep emission to a recombination of a bound electron with a free hole. Hence, we can attribute the determined $E_{A2}$ of 150 meV to an ionization energy of this deep donor for Cu-poor ([Cu]/[In]* ∼ 0.972) CIS. At the same time, the $E_{A2}$ of 27 meV is too small for this electron emission process, and we tentatively assign it to an ionization of a competitive nonradiative center for Cu-rich ([Cu]/[In]* ∼ 1.023) CIS. In a second scenario, if the broad

defect band is of acceptor type and located about 0.2 eV above the VB, the deep emission could be explained by the recombination of a free electron and a bound hole. In this case the $E_{A2}$ for Cu-poor CIS corresponds to an ionization energy of this deep acceptor, while $E_{A2}$ for Cu-rich CIS has the same meaning as in the first scenario. Spindler *et al.* found this deep emission to be more intense in Cu-rich samples than in Cu-poor ([Cu]/[In] = 0.8), and we observe that close to [Cu]/[In]* = 1.00 the deep emission is much stronger for slightly Cu-poor compositions. It is interesting to note that the deep defect level at 0.8 eV has also been identified in transient photocapacitance measurements on polycrystalline CIS samples, as well as in $CuGa_xIn_{1-x}Se_2$ samples with $x$ up to 0.8 [34].

In our present study the availability of many measurement points at different—but very close—compositions combines the advantage of better comparability of measurements on a sample from a single deposition process and the variation of [Cu]/[In]* ratio up to the third decimal place. The challenge to pinpoint compositions on this narrow scale is exemplified by an additional as-grown sample without postdeposition annealing. As shown in Fig. S6 [21], the ratio of the Cu-Se and CIS Raman peaks of this sample exhibits a plateau region with an almost constant small signal before a strong increase. We explain this observation by the formation of a thin $Cu_{2-x}Se$ layer on the thin-film surface prior to Cu saturation along the whole thin-film thickness, as modeled previously based on *in situ* EDXRD/XRF and LLS results during CIS deposition [5]. An additional annealing after the deposition provides time for the Cu atoms to diffuse further into the sample, which fits into the more steplike evolution of the signal of the annealed sample in Fig. 1(b). The PL results of the as-grown sample without annealing are shown in the Supplemental Material in Figs. S7 and S8 [21]. Apart from quantitative differences, which can be expected to occur for different samples due to different defect densities, the qualitative evolution of the PL signals is very similar to the above presented results of the annealed sample. Only the 0.985-eV band is not observed in the as-grown sample at the [Cu]/[In]* ratio where it appears in the annealed sample, which might be due to a higher Cu in-depth inhomogeneity in the as-grown sample.

Our results do not show an abrupt change of the recombination mechanism at the transition from a Cu-poor to a Cu-rich composition: at 60 K the radiative recombination is dominated by the deep emission at ~0.8-eV in both composition ranges and at 15 K by the DAP band at 0.97 eV, which is replaced by the DAP band at 0.985 eV only at Cu-poor compositions below [Cu]/[In]* < 0.982. Most strikingly, however, the PL yields $I_{PL}$ of both the 0.97-eV band at 15 K and the 0.8-eV band at 60 K show a similar strong decrease with increasing Cu content [see Figs. 2(b) and 3(b)]. Since the intensity of a DAP transition is proportional to the product $N_A^0 N_D^0$ of neutral acceptor and donor concentrations [22], we assume that the variation in $I_{PL}$ is related to variations in the concentrations of the involved defects.

To interpret the observed dependence of the PL yield on the sample composition, we try to connect the measured emission band with possible point defects. Recently, the formation-energy and the transition-energy levels for a series of intrinsic point defects (vacancies, antisites and interstitials) and defect complexes in CIS were calculated by using screened-exchange hybrid density functional theory [35]. We believe that the results of this study based on hybrid functionals may be more relevant for comparison with experiment than earlier theoretical studies based on local density approximation (LDA) functionals [36,37], as it predicts the band-structure and defect properties in semiconductors more accurately [38]. The theoretical results of Ref. [35] show that the vacancy $V_{Cu}$ is the main shallow acceptor in CIS. Based on this result, we associate the DAP band at 0.985 eV detected at Cu-poor compositions ([Cu]/[In]* < 1) with the recombination of the shallowest acceptor originating from $V_{Cu}$ and the shallowest donor (introduced by a cation antisite $In_{Cu}^{2+}$: an In atom on Cu lattice site in the 2+ charge state). We assign the 0.97-eV band to a transition between the second shallowest acceptor in CIS, which is an antisite $Cu_{In}^{1-}$, and the same shallowest donor. Interestingly, even previous to the theoretical results, the acceptor state of the $Cu_{In}$ antisite or $V_{In}$ vacancy was already suggested in studies where the 0.97-eV band showed properties of the FB transition [13,32]. Because the $Cu_{In}^{2-}$ antisite shows the lowest formation energy and gives rise to a deep acceptor, we attribute the deep band at 0.8 eV to transitions involving this defect, although the calculated defect level of 0.62 eV [35] is significantly larger than the 0.2 eV observed in our experiment. This assignment is in contrast to earlier reports suggesting that indium or copper interstitials [33] or transitions from the indium antisite $In_{Se}$ to the vacancy $V_{In}$ [32] are responsible for the 0.8-eV emission in CIS. These previous assignments are less likely to be valid, as the suggested point defects have very high formation energies [35]. A recent review of the electronic defect properties supports our assignments of the defect bands to transitions between the intrinsic cation antisite defects of CIGS [16]. Our interpretation concerning the antisite $Cu_{In}$ defects involvement in both PL transitions at 0.97 and 0.8 eV could explain the observed similarity in their PL yields variation on Cu content near [Cu]/[In]* ~ 1.0, as the rate of radiative defect recombination is proportional to the concentration of the involved neutral defects [22]. Since one might intuitively expect more $Cu_{In}$ antisite defects with increasing Cu content, the strong decrease of the PL intensity for both 0.97 and 0.8 eV [see Figs. 2(b) and3(b)] appears surprising at first. However, the formation energy of the [$Cu_{In}$ + $In_{Cu}$] antisite defect complex decreases with lower Cu contents in Cu-poor CIS [39]. Also, it has been shown that planar structural defects, such as stacking faults and twins, abruptly disappear at the transition from a Cu-poor to a Cu-rich composition [4]. While planar structural defects are not directly linked to optical transitions, it was recently shown that Cu accumulates at these defects [12]. These local Cu accumulations result in $Cu_{In}$ antisite defects around stacking faults [12], which would disappear with the stacking faults once the material passes the Cu-poor/Cu-rich transition.

## IV. CONCLUSIONS

In summary, we found from the combined application of Raman and temperature-dependent PL measurements on $CuInSe_2$ close to the Cu saturation point that on both sides of the composition transition the radiative recombination is dominated by the donor-acceptor pair emission at 0.97 eV

and a deep emission at 0.8 eV, which has previously not been described in detail. A combination of *in situ* process control during sample preparation with Raman and XRF measurements provides a precise relative determination of the lateral composition gradient, which allows determining the photoluminescence yield as a function of very small composition variations. For both emissions we observe a strong decrease of the PL emission intensity with increasing Cu concentration up to the point of Cu saturation. Based on previous density functional theory results, we associate the defect PL bands at 0.97 and 0.8 eV with the antisite $Cu_{In}$ defect in 1- and 2-charge states, respectively. We therefore suggest that the observed strong decrease of the PL emission intensity on the Cu-rich side of the gradient sample might be explained by a decrease of $Cu_{In}$ antisite defects.

With respect to improving the performance of $CuInSe_2$ solar cells, the identification of main nonradiative centers is essential. Since the 0.8-eV defect transition is relatively deep, a significant nonradiative recombination activity is expected for the associated defects. This defect may play an important role in limiting the open-circuit voltage in $CuInSe_2$ devices, and further investigations of how this defect can be avoided should be performed.

## ACKNOWLEDGMENTS

This research was financially supported by the Helmholtz Virtual Institute's "Microstructure Control for Thin-Film Solar Cells" (VH-VI-520), by the German Federal Ministry for Economic Affairs and Energy (BMWi) via the project EFFCIS (0324076B), and by the EMPIR program cofinanced by the Participating States and from the European Union's Horizon 2020 Research and Innovation Program via the project HyMET. We thank Anja Scheu, Jakob Lauche, Tim Münchenberg, Juan Dominguez, Jan-Peter Bäcker, and Phillip Loche for their support with the sample preparation. Thanks also go to Manuela Klaus, Christoph Genzel, Matthias Meixner, Daniel Apel, and Guido Wagner for support at the EDDI beamline at the BESSY II Synchrotron.

[1] Solar Frontier Achieves World Record Thin-Film Solar Cell Efficiency of 23.35%, accessed on January 17, 2019; http://www.solar-frontier.com/eng/news/2019/0117_press.html.

[2] M. A. Contreras, J. R. Tuttle, A. Gabor, A. Tennant, K. Ramanathan, S. Asher, A. Franz, J. Keane, L. Wang, J. Scofield, and R. Noufi, in *Proceedings of the 24th IEEE Photovoltaic Specialist Conference* (IEEE, New York, 1994), p. 68.

[3] A. M. Gabor, J. R. Tuttle, D. S. Albin, M. A. Contreras, R. Noufi, and A. M. Hermann, Appl. Phys. Lett. **65**, 198 (1994).

[4] R. Mainz, E. Simsek Sanli, H. Stange, D. Azulay, S. Brunken, D. Greiner, S. Hajaj, M. D. Heinemann, C. A. Kaufmann, M. Klaus, Q. M. Ramasse, H. Rodriguez-Alvarez, A. Weber, I. Balberg, O. Millo, P. A. van Aken, and D. Abou-Ras, Energy Environ. Sci. **9**, 1818 (2016).

[5] R. Mainz, H. Rodriguez-Alvarez, M. Klaus, D. Thomas, J. Lauche, A. Weber, M. D. Heinemann, S. Brunken, D. Greiner, C. A. Kaufmann, T. Unold, H. W. Schock, and C. Genzel, Phys. Rev. B. **92**, 155310 (2015).

[6] H. Stange, S. Brunken, H. Hampel, H. Rodriguez-Alvarez, N. Schäfer, D. Greiner, A. Scheu, J. Lauche, C. A. Kaufmann, T. Unold, D. Abou-Ras, and R. Mainz, Appl. Phys. Lett. **107**, 152103 (2015).

[7] M. D. Heinemann, R. Mainz, F. Österle, H. Rodriguez-Alvarez, D. Greiner, C. A. Kaufmann, and T. Unold, Sci. Rep. **7**, 45463 (2017).

[8] E. Simsek Sanli, Q. M. Ramasse, R. Mainz, A. Weber, D. Abou-Ras, W. Sigle, and P. A. van Aken, Appl. Phys. Lett. **111**, 032103 (2017).

[9] H. Stange, S. Brunken, D. Greiner, M. D. Heinemann, C. A. Kaufmann, S. S. Schmidt, J. P. Bäcker, M. Klaus, C. Genzel, and R. Mainz, Acta Mater. **111**, 377 (2016).

[10] H. Stange, S. Brunken, D. Greiner, M. D. Heinemann, D. Barragan-Yani, L. A. Wägele, C. Li, E. Simsek Sanli, M. Kahnt, S. S. Schmidt, J. P. Bäcker, C. A. Kaufmann, M. Klaus, R. Scheer, C. Genzel, and R. Mainz, J. Appl. Phys. **125**, 035303 (2019).

[11] E. Simsek Sanli, Q. M. Ramasse, W. Sigle, D. Abou-Ras, R. Mainz, A. Weber, H.-J. Kleebe, and P. A. van Aken, J. Appl. Phys. **120**, 205301 (2016).

[12] E. Simsek Sanli, D. Barragan-Yani, Q. M. Ramasse, K. Albe, R. Mainz, D. Abou-Ras, A. Weber, H. J. Kleebe, and P. A. van Aken, Phys. Rev. B. **95**, 195209 (2017).

[13] S. Zott, K. Leo, M. Ruckh, and H. W. Schock, J. Appl. Phys. **82**, 356 (1997).

[14] A. Bauknecht, S. Siebentritt, J. Albert, and M. C. Lux-Steiner, J. Appl. Phys. **89**, 4391 (2001).

[15] B. M. Keyes, P. Dippo, W. K. Metzger, J. Abushama, and R. Noufi, J. Appl. Phys. **94**, 5584 (2003).

[16] C. Spindler, F. Babbe, M. H. Wolter, F. Ehré, K. Santhosh, P. Hilgert, F. Werner, and S. Siebentritt, Phys. Rev. Mater. **3**, 090302 (2019).

[17] F. Babbe, H. Elanzeery, M. H. Wolter, K. Santhosh, and S. Siebentritt, J. Phys.: Condens. Matter **31**, 425702 (2019).

[18] H. Rodriguez-Alvarez, A. Weber, J. Lauche, C. A. Kaufmann, T. Rissom, D. Greiner, M. Klaus, T. Unold, C. Genzel, H. W. Schock, and R. Mainz, Adv. Energy Mater. **3**, 1381 (2013).

[19] R. Scheer, A. Pérez-Rodríguez, and W. K. Metzger, Prog. Photovolt. **18**, 467 (2010).

[20] H. Tanino, T. Maeda, H. Fujikake, H. Nakanishi, S. Endo, and T. Irie, Phys. Rev. B **45**, 13323 (1992).

[21] See Supplemental Material at http://link.aps.org/supplemental/10.1103/PhysRevMaterials.4.064605 for XRF data of CIS samples, additional PL results of the annealed CIS sample, and Raman and PL data of the as-grown CIS sample.

[22] T. Schmidt, K. Lischka, and W. Zulehner, Phys. Rev. B **45**, 8989 (1992).

[23] P.W. Yu, J. Appl. Phys. **47**, 677 (1976).

[24] J. Krustok, A. J. Agi, J. Raudoja, and M. Altosaar, Sol. Energy Mater. Sol. Cells **79**, 401 (2003).

[25] S. Siebentritt, N. Rega, A. Zajogin, and M. C. Lux-Steiner, Phys. Status Solidi C **1**, 2304 (2004).
[26] L. Gütay, D. Regesch, J. K. Larsen, Y. Aida, V. Depredurand, A. Redinger, S. Caneva, S. Schorr, C. Stephan, J. Vidal, S. Botti, and S. Siebentritt, Phys. Rev. B **86**, 045216 (2012).
[27] S. Levcenko, H. Stange, L. Choubrac, D. Greiner, M. D. Heinemann, R. Mainz, and T. Unold, J. Appl. Phys. **127**, 125701 (2020).
[28] F. Luckert, M. V. Yakushev, C. Faugeras, A. V. Karotki, A. V. Mudryi, and R. W. Martin, J. Appl. Phys. **111**, 093507 (2012).
[29] V. Deprédurand, T. Bertram, D. Regesch, B. Henx, and S. Siebentritt, Appl. Phys. Lett. **105**, 172104 (2014).
[30] J. Krustok, H. Collan, and K. Hjelt, J. Appl. Phys. **81**, 1442 (1997).
[31] E. Zacks and A. Halperin, Phys. Rev. B **6**, 3072 (1972).
[32] C. Rincón, S. M. Wasim, E. Hernández, M. A. Arsene, F. Voillot, J. P. Peyrade, G. Bacquet, and A. Albacete, J. Phys. Chem. Solids **59**, 245 (1998).
[33] M. V. Yakushev, A. V. Mudryi, V. F. Gremenok, E. P. Zaretskaya, V. B. Zalesski, Y. Feofanov, and R. W. Martin, Thin Solid Films **451-452**, 133 (2004).
[34] J. T. Heath, J. D. Cohen, W. N. Shafarman, D. X. Liao, and A. A. Rockett, Appl. Phys. Lett. **80**, 4540 (2002).
[35] J. Pohl and K. Albe, Phys. Rev. B **87**, 245203 (2013).
[36] S. B. Zhang, S. H. Wei, A. Zunger, and H. Katayama-Yoshida, Phys. Rev. B **57**, 9642 (1998).
[37] C. Domain, S. Laribi, S. Taunier, and J. Guillemoles, J. Phys. Chem. Solids **64**, 1657 (2003).
[38] C. Freysoldt, B. Grabowski, T. Hickel, J. Neugebauer, G. Kresse, A. Janotti, and C. G. Van de Walle, Rev. Mod. Phys. **86**, 253 (2014).
[39] D. Huang and C. Persson, J. Phys.: Condens. Matter **24**, 455503 (2012).